Rigorous experimental confirmation of a theoretical model for diffusion-limited oxidation

Kenneth T. Gillen* and Roger L. Clough
Sandia National Laboratories, Albuquerque, NM 87185, USA
(Received 9 May 1991; accepted 12 February 1992)

A rigorous test of theoretical treatments for diffusion-limited oxidation was completed by conducting an extensive series of radiation-initiated oxidation experiments on a commercial EPDM material. Oxidation profiles were monitored from density changes; profiles were obtained *versus* sample thickness, radiation dose rate and surrounding oxygen partial pressure. The resulting profile shapes and magnitudes could be quantitatively fit with a two-parameter theoretical treatment based on oxidation kinetics containing unimolecular termination reactions. The theoretical parameters derived from fitting allowed quantitative confirmation of a governing theoretical expression relating these parameters to independently measured values for the oxygen consumption and permeation rates.

(Keywords: oxidation; diffusion; ageing; degradation; kinetics; EPDM; profile; radiation)

INTRODUCTION

When polymers are aged in air, complications caused by diffusion-limited oxidation effects can impact attempts to quantitatively understand oxidation processes and to extrapolate accelerated exposures to long-term conditions. Diffusion-limited oxidation effects result when the rate of oxygen consumption in a material during ageing is greater than the rate at which oxygen can be resupplied from the surrounding air atmosphere by diffusion processes. This leads to a reduction in the dissolved oxygen concentration in the interior of the material which can yield reductions in the oxidation rate in these regions. Since the rate of oxidation at the surfaces of the material will remain at the equilibrium value, such diffusion-limited effects will lead to a heterogeneously oxidized material having oxidized regions near the air-exposed surfaces and regions with reduced or minimal oxidation towards the sample interior. Given that this effect is quite commonly observed in various air environments (e.g. thermal, u.v., high energy radiation), a number of theoretical treatments of diffusion-limited oxidation have been published[1–7]. The theories predict that the importance of diffusion-limited oxidation will depend upon the material thickness, the rate at which oxygen is consumed during ageing, the oxygen permeability coefficient and the oxygen partial pressure surrounding the sample during ageing. To obtain tractable solutions, all of the theoretical approaches assume that time-independent values apply for the permeability coefficient, the oxygen consumption rate and the partial pressure; this allows steady-state solutions to be generated.

There are a number of useful experimental techniques for monitoring diffusion-limited oxidation profiles[6,8–15]. If experimental and theoretical profiles can be compared, the theories can be verified and then confidently used to predict the importance of diffusion effects prior to the initiation of ageing tests. Rigorous testing of the theoretical approaches requires: (1) finding a material which can be aged under conditions in which the oxygen permeability coefficient and the oxygen consumption rate are known and are approximately independent of time; (2) matching the shapes and magnitudes of the theoretical profiles with experimental profiles obtained as a function of sample thickness, initiation rate and surrounding oxygen pressure; and (3) confirming that the theoretical parameters derived from the matching procedure are consistent with the independently measured values of the permeability coefficient and consumption rate. This paper summarizes what we believe is the first complete quantitative experimental confirmation of a diffusion-limited oxidation theory.

EXPERIMENTAL

Material

The commercial EPDM material used for these studies was supplied by Parker Seal Group and is designated as E740-75. It is a peroxide-cured terpolymer of ethylene and propylene in approximately equal amounts plus ~3% hexadiene; the formula contains ~35 wt% carbon black and a free radical scavenger antioxidant. It was obtained as compression moulded sheets (15 cm × 15 cm) in several thicknesses.

* To whom correspondence should be addressed

0032-3861/92/204358-08

Radiation ageing

Combined radiation–thermal exposures were carried out in an underwater ^{60}Co ageing facility using water-tight ageing cans (~ 1 litre volume), an arrangement that facilitated long-term exposures. By selecting positions relative to the ^{60}Co pencils, dose rates ranging from ~ 100 to 7000 Gy h^{-1} (10–700 krad h^{-1}) were available for the current experiments. Uncertainties in the dose rates are estimated to be $\pm 10\%$. Can temperatures were kept at $70 \pm 0.5°C$ during the radiation exposures. A slow, steady flow (~ 30 cm^3 min^{-1}) of either air (21% oxygen), 2% oxygen/98% nitrogen or nitrogen was supplied to each can throughout the experiment. A detailed description of the ageing facility has been published elsewhere[16].

Density profiling

Details of the density profiling technique have been published previously[6]. The technique is based on the use of a density gradient column to obtain the density of successive thin slices across a sample. It depends on the fact that oxidation reactions often lead to substantial and easily measurable increases in polymer density. For the current material (nominal unaged density ~ 1.12 g cm^{-3}), gradient columns were made with a density range from ~ 1.10 to 1.15 g cm^{-3} using $Ca(NO_3)_2$–H_2O solutions. The experimental uncertainty for a single density measurement is estimated to be $< \pm 0.0004$ g cm^{-3}.

Measurements of oxygen consumption and hydrogen production

In order to determine the amount of oxygen consumed and hydrogen produced for irradiated EPDM samples, measured quantities of material were initially sealed with known amounts of oxygen in a number of glass containers. The containers were then aged at 70°C in combination with a selected dose rate ranging from 120 to 2080 Gy h^{-1}. After exposure, a Tracor MT150g gas chromatograph, equipped with a molecular sieve column and a thermal conductivity detector, was used to determine the amounts of oxygen and hydrogen in the tube. Both gases were quantified using primary standards. In general, the oxygen consumption rate will depend on the oxygen partial pressure surrounding the material. Since the analysis below will require an estimate of the consumption rate under air-ageing conditions (~ 13.2 cmHg oxygen partial pressure in Albuquerque), and since the experimental procedure requires a measurable drop in oxygen pressure, attempts were made to select the ratio of sample weights to cell volumes such that the average of the initial and final oxygen pressures was reasonably close to the desired 13.2 cmHg value. For the seven reported consumption runs, the initial and final oxygen partial pressures in the cells averaged 16.1 and 6.4 cmHg, respectively.

Oxygen permeation measurements

A sheet of the EPDM material (1.04 mm thick) was sent to Mocon Modern Controls, Inc. of Minneapolis where oxygen permeation constants were measured at 23 and 60°C. The instrument is based on the ASTM standard test method D-3985-81. To avoid detector saturation, the measurements were conducted with a test gas containing 0.5% oxygen.

THEORETICAL MODELLING OF DIFFUSION-LIMITED OXIDATION

In order to quantitatively model diffusion-limited oxidation profiles, one must combine expressions for oxygen consumption with diffusion equations. To derive oxygen consumption rates, detailed knowledge of the kinetics of oxidation must exist, a difficult requirement given the complexities of oxidation processes in polymers[17]. In the earlier theoretical treatments, the kinetic rate expressions were greatly simplified by assuming either that the oxygen consumption rate was linearly proportional to the oxygen concentration[1–4], or that it was independent of the oxygen concentration[1]. Although these models may hold in the limiting cases of very low and very high oxygen concentrations, respectively, the consumption rate of interest to most materials would be expected to have a more complex dependence on the oxygen concentration. Recently, two more general models were derived based on a more detailed look at the kinetics[5–7]. These models assume that the following kinetic scheme[18,19] represents a reasonable first-order approximation for the oxidation of organic materials in various environments (thermal, mechanical, u.v. light, ionizing radiation, etc.).

Initiation	$\text{Polymer} \xrightarrow{R_i} \text{R}^{\cdot}$		(1)
Propagation	$\text{R}^{\cdot} + \text{O}_2 \xrightarrow{k_2} \text{RO}_2^{\cdot}$		(2)
	$\text{RO}_2^{\cdot} + \text{RH} \xrightarrow{k_3'} \text{ROOH} + \text{R}^{\cdot}$		(3)
Bimolecular termination	$\text{R}^{\cdot} + \text{R}^{\cdot} \xrightarrow{k_4} \text{Products}$		(4)
	$\text{RO}_2^{\cdot} + \text{R}^{\cdot} \xrightarrow{k_5} \text{Products}$		(5)
	$\text{RO}_2^{\cdot} + \text{RO}_2^{\cdot} \xrightarrow{k_6} \text{Products} + \text{O}_2$		(6)
Unimolecular termination	$\text{RO}_2^{\cdot} \xrightarrow{k_7} \text{Products}$		(7)
	$\text{R}^{\cdot} \xrightarrow{k_8} \text{Products}$		(8)
Branching	$\text{ROOH} \xrightarrow{k_9} \text{RO}^{\cdot} + {}^{\cdot}\text{OH}$		(9)

Environmental differences occur mainly in the details of the free radical producing initiation step. It is particularly easy to control the initiation rate in the γ-initiated case, since R_i is typically independent of ageing time and linear with the radiation dose rate. In addition, branching reactions, which may complicate the oxidation processes occurring at the high temperatures used for thermal oxidation studies, are often unimportant for lower temperature, relatively short-term γ-initiated oxidation. Any growth in importance of branching reactions as degradation proceeds will cause the oxidation rate to increase with time, further complicating attempts at quantitative modelling. For these reasons, γ-initiated oxidation is the best choice for initial attempts at quantitatively modelling diffusion-limited oxidation effects. Complications, such as time-dependent oxidation rates, may then be addressed once confidence exists in models derived for the simpler situations.

For γ-initiated oxidations involving moderate temperatures, we will therefore assume that the chemistry is adequately represented by reactions (1)–(8). The scheme involving the bimolecular termination steps [reactions (1)–(6)], originally derived for the oxidation of organic liquids, has been invoked for many years for explaining the oxidation of polymers. Using a steady-state analysis

and assuming long kinetic chain lengths (many propagation cycles compared to termination reactions) and $k_5^2 = 4k_4k_6$, the oxygen consumption rate is given by[14]:

$$\frac{dO_2}{dt} = \frac{C_{1b}[O_2]}{1 + C_{2b}[O_2]} \quad (10)$$

where the constants C_{1b} and C_{2b}, appropriate to the bimolecular theory, are given by:

$$C_{1b} = \frac{k_2 R_i^{0.5}}{(2k_4)^{0.5}} \quad \text{and} \quad C_{2b} = \frac{k_6^{0.5} k_2}{k_4^{0.5} k_3} \quad (11)$$

and $k_3 = k_3'[RH]$.

For many polymeric materials, unimolecular termination reactions are often found to be dominant. For instance, in the presence of sufficient radical scavenger antioxidant, the radical species ($RO_2^{\cdot}$ and $R^{\cdot}$) can terminate in pseudo first-order reactions, yielding an oxidation scheme consisting of reactions (1)–(3) plus (7) and (8). The rate of oxidation is then given by[6,7]:

$$\frac{dO_2}{dt} = \frac{C_{1u}[O_2]}{1 + C_{2u}[O_2]} \quad (12)$$

This expression is identical in form to the bimolecular result given in equation (10), except that the constants C_{1u} and C_{2u} from the unimolecular analysis are given by:

$$C_{1u} = \frac{k_2 R_i}{k_8} \quad \text{and} \quad C_{2u} = \frac{k_2 k_7}{k_8(k_3 + k_7)} \quad (13)$$

Although the bimolecular and unimolecular schemes yield oxygen consumption rates that have identical functional dependencies on the oxygen concentration, their dependencies on the initiation rate, R_i, are quite different (half- and first-order, respectively). Thus, when data at various initiation rates are available, one can easily distinguish between the two schemes. It is also of interest to note from equations (10) and (12) that the oxygen consumption rate becomes proportional to, and independent of, the oxygen concentration at low and high oxygen concentrations, respectively; these limits correspond to the assumptions used in the earlier theoretical treatments of diffusion-limited oxidation[1–4].

Cunliffe and Davis[5] used the bimolecular kinetic expression for oxygen consumption and showed that it could be combined with standard diffusion expressions[20] to derive theoretical oxidation profiles for slabs of material of thickness L. Their analysis assumed one-dimensional diffusion (L much smaller than the other two slab dimensions), Fickian behaviour and time-independent values for: (1) the oxygen consumption rate; (2) the oxygen permeability coefficient; and (3) the oxygen partial pressure surrounding the sample. Their steady-state results depended on two parameters, α and β, given by:

$$\alpha = C_1 L^2/D \quad \text{and} \quad \beta = C_2 Sp = C_2[O_2]_e \quad (14)$$

where D and S are the oxygen diffusion and solubility parameters in the material, p is the oxygen partial pressure of the surrounding atmosphere, $[O_2]_e$ denotes the dissolved oxygen concentration at the edge of the sample and C_1 and C_2 are the bimolecular constants C_{1b} and C_{2b} given in equation (11). *Figures 1–3* give representative theoretical results for small, intermediate and large values of β. The left-hand side[6,7] of each figure plots profiles of Θ_i, the steady-state oxygen concentration

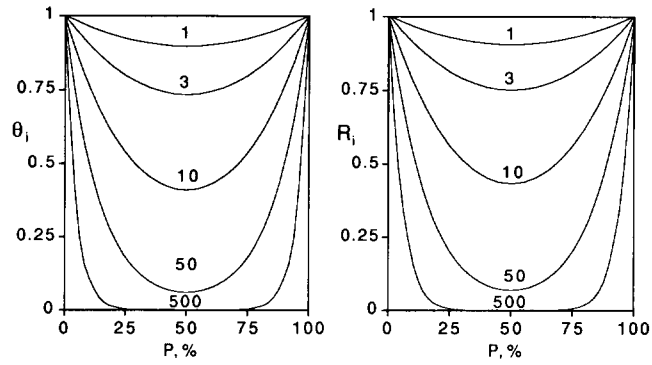

Figure 1 Theoretical oxygen concentration[6,7] (Θ_i) and oxidation[5] (R_i) profiles for various values of α (indicated on figure) with $\beta = 0.1$. P represents the percentage of the distance from one oxygen-exposed surface of the slab of material to the opposite oxygen-exposed surface

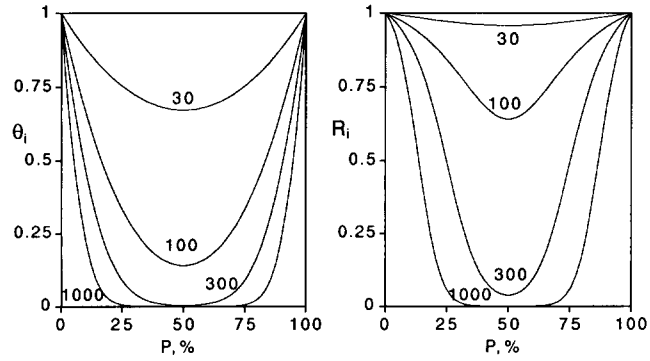

Figure 2 Identical to *Figure 1* except that $\beta = 10$

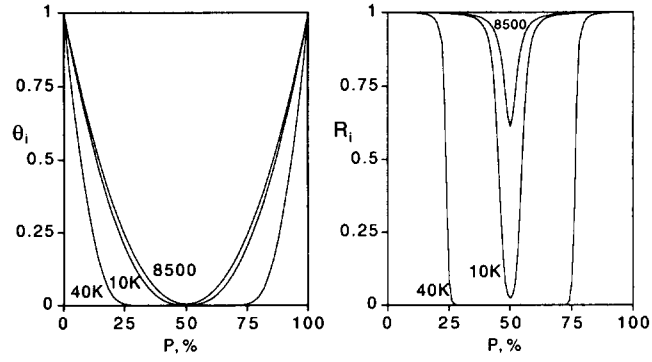

Figure 3 Identical to *Figure 1* except that $\beta = 1000$

(normalized to the equilibrium value at the sample surface) for representative values of α; the right-hand side[5] plots corresponding profiles of R_i, the steady-state normalized oxidation rate. P gives the percentage of the distance from one oxygen-exposed surface of the slab to the opposite oxygen-exposed surface. For small values of β, the oxidation is proportional to the oxygen concentration, yielding 'U-shaped' profiles. When β is large, oxidation is insensitive to oxygen concentration until the latter has dropped significantly, resulting in 'step-shaped' profiles. For intermediate values of β, profile shapes of intermediate character result. If experimental data can be used to generate values of α and β, the following theoretical relationship[5] can be tested:

$$R_0 L^2/(pP_{ox}) = \alpha/(\beta + 1) \quad (15)$$

where R_0 represents the equilibrium oxygen consumption rate and P_{ox} is the oxygen permeability coefficient for the material.

In deriving the above theoretical profiles, the bimolecular result for the oxygen consumption rate, given by equation (10), was combined with standard diffusion equations. Since the unimolecular consumption rate, given in equation (12), has an identical dependence of oxygen consumption on oxygen concentration, the same theoretical profiles and the theoretical relationship given by equation (15) also hold for the unimolecular case[6,7], except that C_{1u} and C_{2u} are substituted for C_1 and C_2 in equation (14). In fact, the only method of distinguishing between the bimolecular and unimolecular theories is to experimentally test the fits *versus* initiation rate. This is clear since α is proportional to C_1, which is first order in R_i for the unimolecular model and half-order in R_i for the bimolecular model.

QUANTITATIVE TESTS OF THE THEORETICAL OXIDATION PROFILES

The above theories will now be quantitatively tested. This first involves determining whether the shapes of experimental oxidation profiles plus their dependence on sample thickness L, initiation rate R_i and oxygen pressure p can adequately fit with either theoretical treatment. If this can be verified, the theoretical fit parameters, α and β, together with independently derived values of the oxygen consumption (R_0) and permeation (P_{ox}), can then be used to test the theoretical relationship given by equation (15). Since the theory was derived assuming a time-independent R_0 and a time-independent P_{ox} during ageing, a successful validation requires a system in which R_0 and P_{ox} are known and are relatively constant with ageing time. For a number of reasons, this assumption often breaks down for oven ageing situations, especially for elastomeric materials[21]. For one thing, thermal ageing can lead to significant increases in modulus values with corresponding decreases in oxygen permeation rates. In addition, oxygen consumption rates usually increase with ageing time, sometimes significantly after a so-called induction period. The time-dependent increase of the consumption rate often correlates with important branching reactions, as denoted by reaction (9) above.

In contrast to thermal ageing situations, the time-independent assumptions often hold in high energy radiation environments[1,2]. In addition, based on an extensive study of several polyethylene, ethylene propylene rubber, EPDM, chlorosulphonated polyethylene, chlorinated polyethylene and chloroprene rubber materials, it is apparent[22] that P_{ox} values seldom change by >10–20% for doses of 0.5 MGy.

Oxygen consumption and permeability coefficient results

With the above in mind, the EPDM rubber was studied using compression moulded sheets of material in three thicknesses (3.02, 1.8 and 0.8 mm). To first assure that the theory is tested at radiation doses low enough to guarantee reasonably time-independent oxygen consumption rates, oxygen consumption experiments were run at a number of radiation dose rates at 70°C. *Table 1* summarizes the dose rates and doses used for each experiment plus the amount of oxygen consumed per cm^3 of material.

In order to derive valid oxygen consumption results, these experiments were run under conditions guaranteed to generate homogeneously rather than heterogeneously oxidized samples. In other words, the materials being studied must be sufficiently thin so as to assure that the measured consumption will not be reduced relative to the true consumption value by diffusion-limited oxidation effects. *Table 1* summarizes the thicknesses used for the seven consumption runs. In a later section, it is shown that diffusion-limited oxidation effects are unimportant for these particular experiments.

The oxygen consumption results from *Table 1* are plotted in *Figure 4*. The approximately linear behaviour of the 1.22 kGy h^{-1} results out to ~ 0.4 MGy, coupled with a similar consumption rate per Gy at 10 times lower dose rate offer preliminary evidence for the absence of dose–rate effects (e.g. the unimolecular model). We will, in fact, assume that the consumption rate is independent of dose rate (unimolecular kinetics), thereby using the *Table 1* results to obtain the oxygen consumption rate under the conditions of interest for testing equation (15). Further evidence supporting this preliminary indication for the lack of dose–rate effects and hence for the unimolecular model, will be presented below.

Since the slope of the curve at any dose represents the

Table 1 Summary of oxygen consumption experiments

Dose rate (Gy h^{-1})	Dose (MGy)	ΔO_2 (mol O_2 cm^{-3})	$\phi(O_2)$ (mol O_2 cm^{-3} Gy^{-1})	$\phi(H_2)^a$ (mol H_2 cm^{-3} Gy^{-1})	R_0 (mol O_2 cm^{-3} s^{-1})	Sample thickness (mm)	L_c^b (mm)
120	0.0397	2.26×10^{-5}	5.69×10^{-10}	1.57×10^{-10}	4.24×10^{-7}	3.0	13.0
1220	0.203	1.09×10^{-4}	5.36×10^{-10}	2.09×10^{-10}	4.07×10^{-6}	0.8	3.2
1220	0.291	1.64×10^{-4}	5.64×10^{-10}	1.20×10^{-10}	4.28×10^{-6}	0.8	3.2
1220	0.410	2.36×10^{-4}	5.76×10^{-10}	1.76×10^{-10}	4.37×10^{-6}	0.8	3.2
1220	0.495	3.15×10^{-4}	6.36×10^{-10}	1.14×10^{-10}	4.83×10^{-6}	0.8	3.1
2080	0.659	4.64×10^{-4}	7.04×10^{-10}	1.74×10^{-10}	9.11×10^{-6}	<0.5	2.4
2080	1.110	1.33×10^{-3}	1.12×10^{-9}		1.45×10^{-5}	<0.5	1.6

[a] $\phi(H_2)_{av} = 1.58 \pm 0.3 \times 10^{-10}$ for this commercial EPDM (EPDM-C). Since the formulation is ~ 35 wt% carbon black (density ~ 2.25 g cm^{-3}), the base EPDM polymer (EPDM-B), of density ~ 0.86 g cm^{-3}, will represent $\sim 83\%$ of the commercial material's volume, implying that its G value is given by:

$$G(\text{EPDM-B}) = 1.58 \times 10^{-10} \frac{\text{cm}^3\,(\text{EPDM-C})}{0.83\ \text{cm}^3\,(\text{EPDM-B})} \times \frac{\text{cm}^3\,(\text{EPDM-B})}{0.86\ \text{g}\,(\text{EPDM-B})} \times 9.66 \times 10^9 = 2.1 \pm 0.4$$

This value of $G(H_2)$ compares favourably to reported literature values ranging from 1.8 to 2.8 for various EPDM materials[27]

[b] From equation (22) using average values of p and R_0 during the experiment

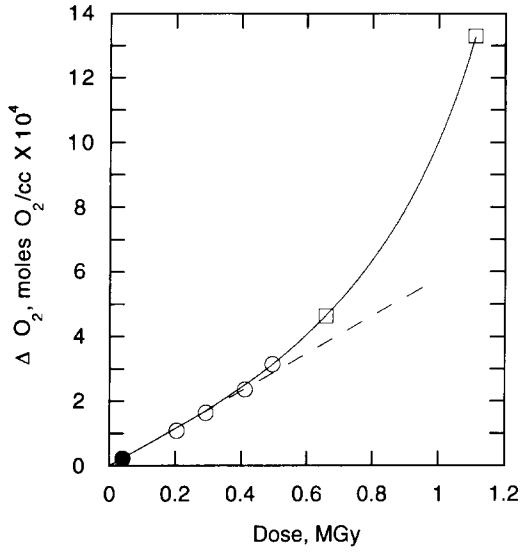

Figure 4 Plot of the oxygen consumption data from *Table 1 versus* radiation dose: (●) 0.12 kGy h^{-1}; (○) 1.22 kGy h^{-1}; (□) 2.08 kGy h^{-1}. The slope of the broken line is 5.6×10^{-10} mol O_2 Gy^{-1} cm^{-3}

instantaneous value of the oxygen consumption rate, the results indicate that this rate can be considered constant only up to ~400 kGy total dose. To assure that the oxygen consumption rate will remain approximately constant during the radiation exposures of the EPDM samples used to test the theoretical treatments, we will therefore confine our attention to samples that receive < ~400 kGy total dose. In this region the consumption rate R_0 is given by the slope of the broken line in *Figure 4*, e.g.:

$$R_0 = (5.6 \pm 0.2) \times 10^{-10} \text{ mol } O_2 \text{ Gy}^{-1} \text{ cm}^{-3} \quad \text{at } 70°C$$

We also need a value for the oxygen permeation constant P_{ox} at 70°C in order to test the theoretical relationship given in equation (15). The following values of P_{ox} were obtained by a coulometric technique (see Experimental section): 1.2×10^{-9} cm^3 STP cm^{-1} s^{-1} $cmHg^{-1}$ at 23°C and 5.1×10^{-9} cm^3 STP cm^{-1} s^{-1} $cmHg^{-1}$ at 60°C (estimated uncertainties of ±10%). Assuming an Arrhenius temperature dependence (activation energy of 7.7 kcal mol^{-1}), the log of P_{ox} was plotted against the inverse absolute temperature and the results extrapolated the short distance to 70°C, yielding:

$$P_{ox} = (7.2 \pm 0.7) \times 10^{-9} \text{ cm}^3 \text{ STP cm}^{-1} \text{ s}^{-1} \text{ cmHg}^{-1} \quad \text{at } 70°C$$

Although P_{ox} will in general decrease with radiation dose, results on similar EPDM materials[22] indicate that any drop will be minor (on the order of 5%) for the doses used in testing the theory.

Thus, up to the limit of where the theory would be expected to hold for this material (~400 kGy), the left-hand side of equation (15) gives:

$$R_0L^2/(pP_{ox}) = 132L^2I \qquad (16)$$

where L is the sample thickness (in cm) and I is the radiation dose rate (in Gy s^{-1}) used for the experiment.

Density profile fitting

For doses up to ~400 kGy, density changes (predominantly caused by oxidation[10]) were readily measured. The density profile technique[10] was therefore chosen to experimentally monitor diffusion-limited oxidation effects for this material. Density profiles were taken on air-aged samples of various thicknesses (~0.8–3 mm) after 70°C radiation ageing at dose rates ranging from 0.16 to 6.65 kGy h^{-1}. Since small density changes occur under inert ageing conditions, a sample was aged in a nitrogen environment at 70°C to a total dose of 380 kGy. The density increase relative to the unaged material was equal to 5×10^{-4} g cm^{-3}; assuming linear behaviour for the doses used in this study (up to 430 kGy), this predicts a 1.32×10^{-6} g cm^{-3} kGy^{-1} density change in inert environments. The small changes predicted from this analysis were subtracted from the density changes found in the presence of oxygen in order to derive the results given in *Figures 5–7*. The crosses represent the changes due to oxidation *versus* cross-sectional position on the sample; the vertical span of each cross represents the estimated experimental uncertainty while the horizontal span denotes the position and thickness of each slice. *Figures 5* and *6* give results for two different thicknesses (3.02 and 1.8 mm) of sample aged under identical conditions (0.32 MGy dose at 6.65 kGy h^{-1}). *Figure 7* shows data for two samples aged at lower dose rates. The top results are for a 3.02 mm thick sample aged to 0.433 MGy at 0.95 kGy h^{-1}; the bottom data are for a 3.07 mm thick sample aged to 0.304 MGy at 4.54 kGy h^{-1}.

In order to fit the experimental data with the theoretical results, we first note that all of our experiments were conducted isothermally (at 70°C) and under conditions where the oxidation rate is approximately independent of time. We noted above that the oxygen consumption rate appeared to be independent of dose rate; further evidence for this conclusion will be presented below. These observations, coupled with the definition

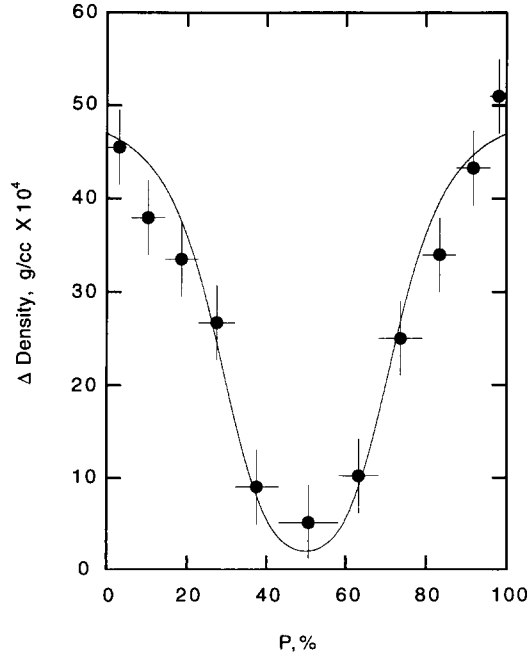

Figure 5 Experimental profiles of density changes (crosses) caused by oxidation for a 3.02 mm thick EPDM sample after ageing in air to a dose of 323 kGy at 6.65 kGy h^{-1} plus 70°C. The curve through the data gives the theoretical fit using the theory parameters $\alpha = 250$ and $\beta = 10$. These values of α and β determine all other values of α and β used for the remaining five profiles in *Figures 6–8* from equations (13) and (14)

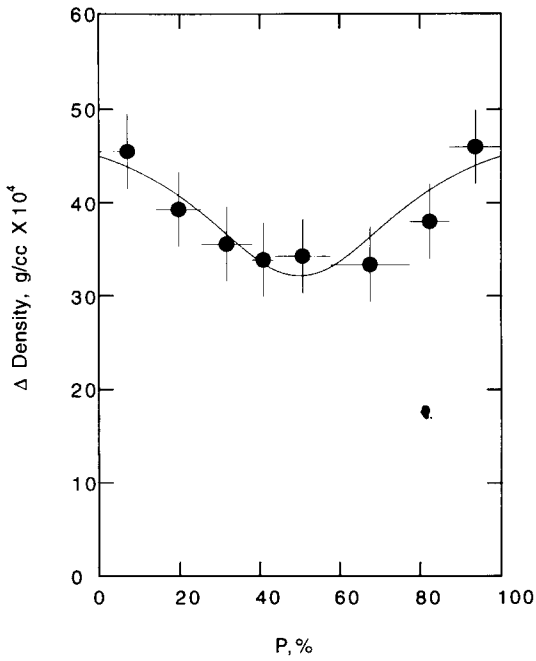

Figure 6 Experimental profiles of density changes (crosses) caused by oxidation for a 1.8 mm thick EPDM sample after ageing in air to a dose of 323 kGy at 6.65 kGy h^{-1} plus 70°C. Except for sample thickness, these ageing conditions are identical to those for the sample shown in *Figure 5*. The curve through the data gives the theoretical fit using the theory parameters $\alpha = 89$ and $\beta = 10$, which are derived with the theory from the values used in *Figure 5*

of β in equation (14), imply that β will be a constant for every air ageing experiment, independent of thickness and dose rate. Thus the same value of β must apply to all four profiles given in *Figures 5–7*. By comparing the general shapes of the four experimental profiles with the theoretical profiles, it is clear that an intermediate value of β will be appropriate. In an earlier preliminary report[23], we showed that optimum theoretical fits to the data of *Figures 5* and *6* occur for $\beta = 6$. However, fairly reasonable fits[7] to these same data can be achieved for values of β ranging from ~3 to 14.

In order to get an improved estimate of the value of β and further test the theory, experiments were carried out at varying oxygen pressure p in the pressure region where the oxidation is sensitive to p. It can be easily seen from either equation (10) or (12) plus equation (14) that the equilibrium oxygen consumption rate (R_0) or equivalently the oxidation rate at the edge of the material (R_e), is given by:

$$R_0 = R_e = \frac{dO_2}{dt} = \frac{C_1[O_2]_e}{1 + C_2[O_2]_e} = \frac{C_1 Sp}{1 + \beta} \qquad (17)$$

Thus, if β_r refers to the value of β at a reference oxygen partial pressure, p_r, the ratio of the edge oxidation rate at an oxygen pressure p, to that under reference conditions, is given by:

$$\frac{R_e(p)}{R_e(p_r)} = \frac{1 + \beta_r}{(p_r/p) + \beta_r} \qquad (18)$$

Given that the preliminary analysis indicated a β of ~7.5 ± 4.5 under the air ageing (reference) conditions, examination of equation (18) shows that lowering the oxygen partial pressure is necessary in order to achieve measurable changes in the edge oxidation rate. We therefore aged samples for 112.5 h at 3.49 kGy h^{-1} and 70°C in a flowing air (21% oxygen) environment and then aged another set of samples under identical conditions in a flowing 2% oxygen environment. To assure that the 2% oxygen samples were initially in equilibrium with oxygen at this concentration, we preswept the ageing can with 2% oxygen for 3 days at room temperature before beginning the radiation exposure. In principle, the required edge oxidation values can be obtained on any thickness of material. However, the use of thick samples combined with the reduced (2%) oxygen environment would be predicted to yield oxidation profiles which drop steeply away from the edges of the sample, thereby reducing the accuracy of the required edge values. For this reason, the thinnest sheets (~0.8 mm thick) of the EPDM material were used for these experiments. *Figure 8* shows the resulting density profiles, with the top data coming from the air-aged samples and the bottom data from the 2% O_2 samples. It is clear that decreasing the oxygen pressure significantly reduced the amount of oxidation. From our estimate that

$$\frac{R_e(p = 2\%\,O_2)}{R_e(p = 20.95\%\,O_2)} = 0.54 \pm 0.06 \qquad (19)$$

equation (18) leads to an estimate of 10 ± 2.5 for β under air-ageing conditions.

With this improved estimate of β, we can now concentrate on deriving values for the second theoretical parameter, α. Given the isothermal nature of our experiments, equation (14) shows that α is proportional to C_1L^2 where C_1 is proportional to either R_i (the dose rate) to the one-half power (bimolecular theory) or to

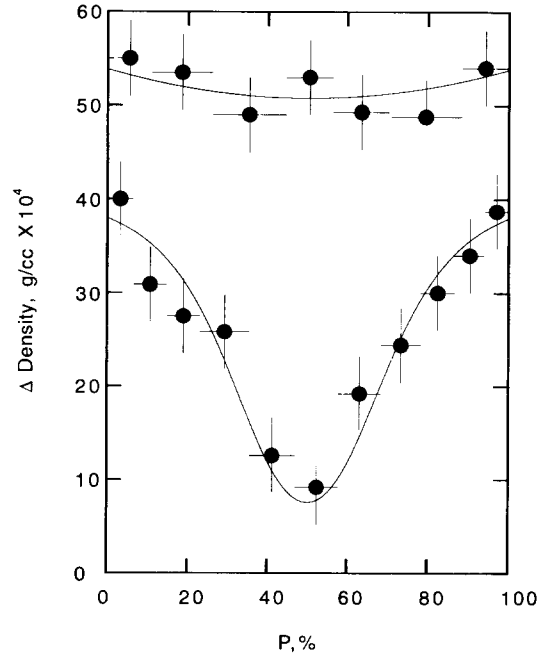

Figure 7 Experimental profiles of density changes (crosses) caused by oxidation at two dose rates which are lower than the dose rate used for the materials shown in *Figures 5* and *6*. The bottom data are for a 3.07 mm sample after ageing in air to a dose of 304 kGy at 4.54 kGy h^{-1} plus 70°C. The top data come from a 3.02 mm thick sample after ageing in air to a dose of 433 kGy at 0.95 kGy h^{-1} plus 70°C. The curves through the data give the theoretical fits using theory parameters of $\alpha = 177$ and $\beta = 10$ for the bottom curve and $\alpha = 35.7$ and $\beta = 10$ for the top curve. These sets of values of α and β are derived with the theory from the values used in *Figure 5*.

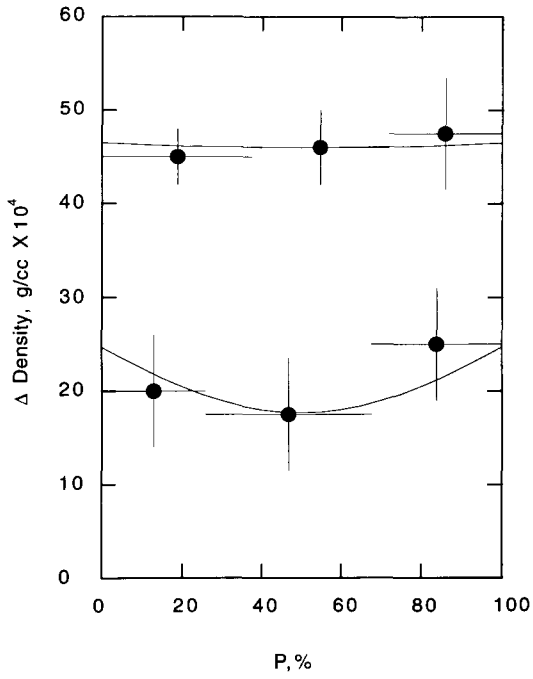

Figure 8 Experimental profiles of density changes (crosses) showing the effect of the surrounding oxygen partial pressure. Both materials were aged to 392 kGy at 3.49 kGy h^{-1} plus 70°C. The top data are for a 0.813 mm thick sample which was aged in air (21% oxygen), whereas the bottom data are for a 0.787 mm thick sample aged in 2% oxygen. The curves through the data give the theoretical fits using theory parameters of $\alpha = 9.5$ and $\beta = 10$ for the top curve and $\alpha = 8.92$ and $\beta = 0.955$ for the bottom curve. These sets of values of α and β are derived with the theory from the values used in *Figure 5*

the first power (unimolecular theory). Thus, once a value of α is fit to any of the six density profiles given in *Figures 5–8*, values of α are determined for the other five profiles. In other words, a two-parameter fit is required where some reference experimental condition is fit with two reference theoretical parameters, α_r and β_r ($=10$ in air for the present experiments), and the values for α and β at all other experimental conditions are calculated from equation (14) together with either equation (10) or equation (12).

It turns out that it is impossible to achieve reasonable fits to either the profile shapes or the edge values of the profiles using the bimolecular theory. On the other hand, use of the unimolecular relationships, given by equations (12) and (14), allows a set of α values to be derived which give consistent agreement between all theoretical and experimental profiles. With $\alpha_r = 250$ for the experiment done in air at 6.65 kGy h^{-1} on the 3.02 mm thick sample, the six resulting theoretical profiles are shown as the solid curves in *Figures 5–8*. Excellent fits *versus* thickness, dose rate and oxygen pressure are obvious.

Additional confirmation of the appropriateness of the unimolecular theory comes from an analysis of the edge values of the profiles. *Figure 9* plots changes in edge density *versus* dose and dose–rate for the five air-aged samples given in *Figures 5–8* and for a number of additional experimental conditions. Within the estimated experimental uncertainties, dose–rate effects are absent for dose rates ranging from 6.65 down to 0.16 kGy h^{-1}. This result is in agreement with the unimolecular theory and further confirms the earlier conclusion about the apparent lack of a dose–rate effect in the oxygen consumption data. It is interesting to note that if the bimolecular theory was appropriate, the change in edge density per dose for the 0.16 kGy h^{-1} experiments would be expected to be $(6.65/0.16)^{0.5} = 6.45$ times greater than that at 6.65 kGy h^{-1}.

Confirmation and use of theoretical expressions

The results clearly show that the two-parameter unimolecular theory for diffusion-limited oxidation does an excellent job of characterizing the profile shapes plus their dependence on thickness, dose–rate and oxygen pressure. Under the reference conditions comprising air-ageing of a 3.02 mm thick sample at 6.65 kGy h^{-1} plus 70°C, α_r and β_r were found to be 250 and 10, respectively, yielding

$$\frac{\alpha}{\beta + 1} = 22.7 \pm 2 \qquad (20)$$

where the estimated uncertainty comes from the range of sets of α and β that can yield reasonable agreement between theory and experiment. We can now compare this result, which represents the right-hand side of the governing theoretical relationship given in equation (15), with the left-hand side. From equation (16) with $L = 0.302$ cm and $I = 1.847$ Gy s^{-1}:

$$R_0 L^2/(pP_{ox}) = 22.2 \pm 3 \qquad (21)$$

This result, which was derived independently from oxygen consumption and permeation measurements, is in excellent agreement with the result derived from the fitting procedures. Not only does this quantitatively confirm the theoretical relationship given by equation (15) but it adds still more confidence to the appropriateness of the theoretical modelling.

Now that we have confidence in the theory, it is of interest to combine the theoretical results together with the theoretical relationship in equation (15) in order to derive a general criterion for estimating when diffusion-limited oxidation effects are important. We define a critical sample thickness L_c as the limiting sample thickness if one wants to guarantee that the integrated

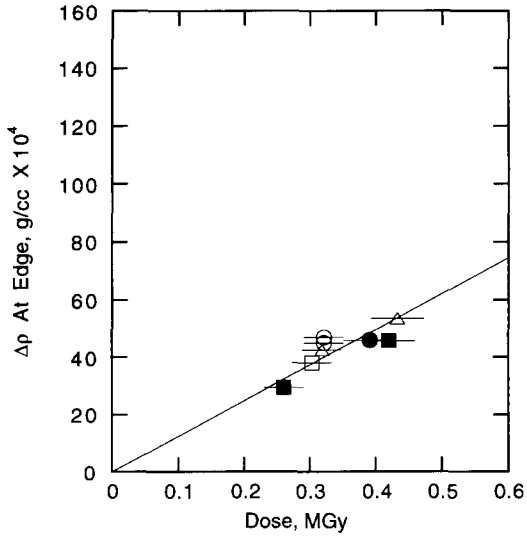

Figure 9 Changes in density at the edges of various samples *versus* total dose at the following dose rates: (○) 6.65 kGy h^{-1}; (□) 4.54 kGy h^{-1}; (●) 3.49 kGy h^{-1}; (△) 0.95 kGy h^{-1}; (■) 0.16 kGy h^{-1}

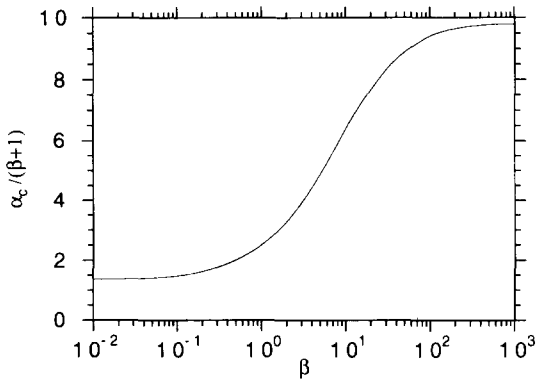

Figure 10 Plot of $\alpha_c/(\beta + 1)$ *versus* β where α_c refers to the value of α corresponding to 90% integrated oxidation

oxidation across the sample will be at least 90% of the homogeneously oxidized case. From equation (15), L_c will be related to α_c (the value of α corresponding to 90% integrated oxidation) by:

$$L_c = \left(\frac{\alpha_c p P_{ox}}{(\beta + 1) R_0} \right)^{0.5} \quad (22)$$

Values of $\alpha_c/(\beta + 1)$ are plotted *versus* β in *Figure 10*; they vary from ~ 1.3 to 9.7 as β varies from low to high values. Some researchers[5,24] have assumed a value of 8, reasonable for large values of β; others[25] have used a value of 1, more reasonable for smaller values of β. In air environments, we find that many commercial polymers tend to have intermediate values of β. Thus, for a material of unknown β, a conservative approach for estimating the maximum allowable thickness in order to be reasonably confident that diffusion-limited oxidation effects are minimal would be to use equation (22) with $\alpha_c/(\beta + 1) = 2$.

Since β in air for the EPDM currently being studied is equal to 10, corresponding to an $\alpha_c/(\beta + 1)$ of ~ 6 from *Figure 10*, values of L_c can be estimated from equation (22) for the experimental conditions used in the oxygen consumption experiments. The results are summarized in *Table 1*. Comparison of these L_c values with the sample thicknesses used for the various consumption experiments (*Table 1*) offers strong evidence that the experiments referred to in *Table 1* were conducted under conditions where homogeneous oxidation occurs.

Since the values of α and β derived for the currently studied EPDM are related to the reaction rate constants underlying the degradation chemistry, the derived values for these parameters can be used to learn something about the kinetics. For instance, it is easy to show that the following relationship holds for the unimolecular oxidation scheme:

$$\frac{R_0}{R_i} = \frac{(k_2 + k_7)}{k_7} \frac{\beta}{(\beta + 1)} \quad (23)$$

The simplest approach[26] to obtaining R_i is to approximate it as twice the hydrogen generation rate, $\phi(H_2)$. From our g.c. measurements, we find that $\phi(H_2)$ is $1.58 \pm 0.3 \times 10^{-10}$ mol H_2 Gy^{-1} cm^{-3}, a value consistent with reported literature values[27] (see footnote in *Table 1*). With a β of 10 in air and $R_0 = 5.6 \times 10^{-10}$ mol O_2 Gy^{-1} cm^{-3}, equation (23) then gives $k_2/k_7 \sim 1$, which implies a low kinetic chain length for radiation ageing in air at 70°C. This is consistent with expectations for a commercially stabilized material since the stabilizer should significantly reduce propagation reactions. By obtaining estimates for D and S, the diffusion and solubility constants for oxygen in this material, estimates of ratios of other rate constants (k_2/k_8 and k_3/k_7) would also be available. However, since the detailed chemistry is unknown and undoubtedly more complex than the oversimplified kinetics used in the derivation[28], we choose not to pursue the rate constant analysis too far.

ACKNOWLEDGEMENTS

This work was performed at Sandia National Laboratories supported by the US Department of Energy under contract number DE-AC04-76DP00789. Able technical assistance was provided by P. D. Silva and G. M. Malone.

REFERENCES

1 Wilson, J. E. *J. Chem. Phys.* 1954, **22**, 334
2 Giberson, R. C. *J. Phys. Chem.* 1962, **66**, 463
3 Jellinek, H. H. G. and Lipovac, S. N. *Macromolecules* 1970, **3**, 237
4 Billingham, N. C. and Walker, T. J. *J. Polym. Sci., Polym. Chem. Edn* 1975, **13**, 1209
5 Cunliffe, A. V. and Davis, A. *Polym. Degrad. Stab.* 1982, **4**, 17
6 Gillen, K. T. and Clough, R. L. in 'Handbook of Polymer Science and Technology' (Ed. N. P. Cheremisinoff), Vol. 2, Marcel Dekker, New York, 1989, pp. 167–202
7 Gillen, K. T and Clough, R. L. *Am. Chem. Soc. Symp. Ser.* 1991, **475**, 457
8 Clough, R. L., Gillen, K. T. and Quintana, C. A. *J. Polym. Sci., Polym. Chem. Edn* 1985, **23**, 359
9 Clough, R. L. and Gillen, K. T. *Am. Chem. Soc. Symp. Ser.* 1984, **280**, 411
10 Gillen, K. T., Clough, R. L. and Dhooge, N. J. *Polymer* 1986, **27**, 225
11 Gillen, K. T., Clough, R. L. and Quintana, C. A. *Polym. Degrad. Stab.* 1987, **17**, 31
12 Gillen, K. T. and Clough, R. L. *Polym. Eng. Sci.* 1989, **29**, 29
13 Jouan, X. and Gardette, J. L. *Polym. Commun.* 1987, **28**, 329
14 Papet, G., Jirackova-Audonin, L. and Verdu, J. *Radiat. Phys. Chem.* 1989, **33**, 329
15 Morita, Y., Yagi, T. and Kawakami, W. *Am. Chem. Soc Symp. Ser.* 1991, **475**, 485
16 Gillen, K. T., Clough, R. L. and Jones, L. H. in 'Investigation of Cable Deterioration in the Containment Building of the Savannah River Nuclear Reactor', Sandia Laboratories Report, SAND81-2613, 1982
17 Grassie, N. and Scott, G. 'Polymer Degradation and Stabilization', Cambridge University Press, Cambridge, 1985
18 Bolland, J. L. *Proc. Roy. Soc.* 1946, **186**, 218
19 Bateman, L. *Quart. Rev. (London)* 1954, **8**, 147
20 Crank, J. 'The Mathematics of Diffusion', Clarendon Press, Oxford, 1975
21 Clough, R. L. and Gillen, K. T. *Polym. Mater. Sci. Eng.* 1988, **58**, 209
22 Seguchi, T. and Yamamoto, Y. in 'Diffusion and Solubility of Oxygen in Gamma Irradiated Polymer Insulation Materials', Japan Atomic Energy Research Inst. Report, JAERI 1299, 1986
23 Gillen, K. T. and Clough, R. L. *Polym. Prepr.* 1990, **31**, 387
24 Seguchi, T., Hashimoto, S., Arakawa, K., Hayakawa, N., Kawakami, W. and Kuriyama, I. *Radiat. Phys. Chem.* 1981, **17**, 195
25 Billingham, N. C. and Calvert, P. D. in 'Developments in Polymer Stabilization' (Ed. G. Scott), Vol. 3, Applied Science, London, 1980, p. 139
26 Decker, C. *J. Polym. Sci., Polym. Chem. Edn* 1977, **15**, 781
27 Arakawa, K. *J. Polym. Sci., Polym. Chem. Edn* 1987, **25**, 1713
28 Gillen, K. T. and Clough, R. L. in 'Irradiation Effects on Polymers' (Eds D. W. Clegg and A. A. Collyer), Elsevier, London, 1991, pp. 157–223